Hyperentanglement-Enabled Direct Characterization of Quantum Dynamics

T. M. Graham,[1] J. T. Barreiro,[2] M. Mohseni,[3] and P. G. Kwiat[1]

[1]*Department of Physics, University of Illinois at Urbana-Champaign, Urbana, Illinois 61801-3080, USA*
[2]*Institut für Experimentalphysik, Universität Innsbruck, Technikerstrasse 25, A-6020 Innsbruck, Austria*
[3]*Research Laboratory of Electronics, Massachusetts Institute of Technology, Cambridge, Massachusetts 02139, USA*

(Received 7 May 2012; published 5 February 2013)

We use hyperentangled photons to experimentally implement an entanglement-assisted quantum process tomography technique known as direct characterization of quantum dynamics. Specifically, hyperentanglement-assisted Bell-state analysis enabled us to characterize a variety of single-qubit quantum processes using far fewer experimental configurations than are required by standard quantum process tomography. Furthermore, we demonstrate how known errors in Bell-state measurement may be compensated for in the data analysis. Using these techniques, we have obtained single-qubit process fidelities over 98% but with one-third the number of experimental configurations required for standard quantum process tomography. Extensions of these techniques to multiqubit quantum processes are discussed.

DOI: 10.1103/PhysRevLett.110.060404 PACS numbers: 03.65.Wj

As scientists advance the frontiers of quantum information science and quantum computing by producing ever larger and more complex quantum systems, there has been an increased need for efficient methods of characterizing quantum states and processes. The information contained in a quantum system may be extracted using state tomography, which is accomplished by making various measurements on multiple copies of the state, and then using these measurement outcomes to reconstruct the density matrix. Similarly, the information describing a quantum process is extracted by probing the process with various quantum states and then making measurements on the output. This characterization, known as process tomography, is generally more difficult than state tomography because quantum processes contain quadratically more information than the states on which they operate. We present an experimental realization of a process tomography technique devised by Mohseni and Lidar [1], known as direct characterization of quantum dynamics (DCQD). DCQD has advantages over other process tomography methods: it requires far fewer experimental settings than techniques which use only local probe states and measurements, and it requires less complicated measurements than techniques requiring a similar number of experimental configurations [2]. In particular, the many-body interactions required by many other entanglement-enhanced process tomography techniques are difficult to implement with any current qubit technology, and physically *impossible* to implement deterministically with linear optics [3–5].

The biggest challenge in applying DCQD for optical qubits is performing the required full Bell measurement on each output state, which is impossible using only linear optics in a restricted Hilbert space [6]. DCQD was implemented with photons using a probabilistic Bell measurement [7]; however, the lack of deterministic Bell measurements meant that more measurements per experimental configuration were required, losing much of the DCQD advantage. We have previously shown that it is possible to perform a complete Bell measurement using quantum systems that are hyperentangled—simultaneously entangled in multiple degrees of freedom—using controlled-NOT (CNOT) logic gates between different degrees of freedom [8]. DCQD using CNOT gates between different degrees of freedom was demonstrated, but only with single-photon *hybrid*-entangled states (entanglement between different degrees of freedom of a single particle) [9]. Because hyperentangled probe states were not used, this technique has a classical interpretation and could as easily have been performed using classical inputs. A deterministic Bell measurement may also be performed using many-body interactions [6]; unfortunately, because optical nonlinear effects are weak, it is impossible to employ nonlinear techniques to perform deterministic Bell measurements on multiphoton states. This limitation is not present in other physical systems, such as ionic spin states. In fact, DCQD with deterministic Bell measurements using many-body interactions has concurrently been demonstrated by Nigg *et al.* [10].

Here we demonstrate DCQD using hyperentanglement-enabled deterministic Bell measurements and techniques that can readily be extended to characterize higher dimensional quantum processes [11]. Specifically, we used photons simultaneously entangled in both polarization and orbital angular momentum to characterize several classes of single-qubit polarization quantum processes using DCQD with one-third the number of experimental configurations that were required using standard quantum process tomography (SQPT). After discussing SQPT methods for comparison, we describe the essential elements of DCQD. Next, we describe our experimental implementation of

both SQPT and DCQD, before discussing possible extensions of the latter.

The information describing a quantum process may be completely parametrized by the χ matrix, which is a representation of a superoperator that maps an input quantum state to an output quantum state; for a single qubit [12],

$$\epsilon(\rho) = \sum_{m,n=0}^{3} \chi_{mn} \sigma_m \rho \sigma_n, \tag{1}$$

where a quantum process ϵ acting on a quantum state ρ can be represented as the sum of transformations made by Pauli matrices σ_m weighted by the elements χ [12]. In SQPT, a state tomography is performed on a complete set of input states [Fig. 1(a)]. SQPT has the advantage of requiring only simple input states and simple measurements. However, this technique requires 12^n experimental configurations to completely characterize a trace-preserving quantum process acting on n qubits [(4^n input states) $\times$ (3^n measurement settings)], which rapidly becomes intractable as n increases [13].

Another type of process tomography—ancilla-assisted process tomography (AAPT)—uses the nonlocal behavior of entangled qubits to decrease the number of necessary inputs to one. Here, the input qubits are entangled with an equal number of ancilla qubits [14]; by performing state tomography on the total quantum state, it is possible to completely reconstruct the quantum process. In fact, by measuring mutually unbiased bases [4] or performing generalized (positive operator-valued measure [15]) measurements instead of just separable state measurements, the AAPT technique can be used to reconstruct the quantum process with far fewer experimental settings than are required by SQPT or even DCQD [2,3,5]. However, the complexity of the measurements required to perform these process tomography techniques increases as the number of qubits n increases, because they require many-body interactions.

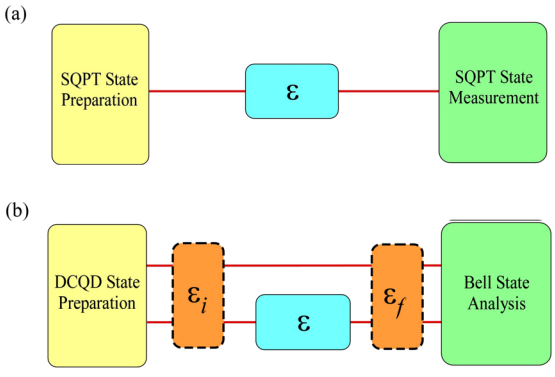

FIG. 1 (color online). The basic measurement schemes for SQPT (a) and DCQD (b) for a single-qubit process ϵ. Though DCQD requires more complex input states and measurement settings than SQPT, it also requires 3 times fewer experimental configurations. The dotted boxes before and after the process in (b) represent errors in source preparation and analysis, here described by initial and final error processes (ϵ_i and ϵ_f).

Unlike SQPT and AAPT, DCQD can *directly* characterize a quantum process without state tomography; the process is characterized by performing complete Bell measurements on a specific set of partially entangled quantum states whose ancilla qubits have interacted with the quantum process [Fig. 1(b)]. In fact, a judicious choice of states also allows one to minimize errors in the process estimation [16]. Not only does the number of experimental settings required by this technique (4^n) scale better than SQPT (12^n), but the most complicated measurement required is a two-qubit Bell measurement, no matter how complicated the process to be measured (i.e., even a four-qubit process requires only pairwise two-qubit Bell measurements).

To investigate how well DCQD works in practice, we used both SQPT and DCQD to measure single-qubit quantum processes acting on polarization. The single- and two-photon polarization states necessary for each respective technique were produced using type I spontaneous parametric down-conversion. Specifically, time-correlated 702-nm photon pairs were created by pumping a pair of β-barium borate (BBO) crystals [11]. In the SQPT measurements, the idler photon heralded the presence of a horizontally polarized signal photon. Liquid crystals prepared the single photons into one of an overcomplete set of probe states [17]: horizontal (H), vertical (V), diagonal (D), antidiagonal (A), left circular (L), and right circular (R). After transmitting each input state through the process, an overcomplete set of measurements was performed on each output state (in the same bases as above) using adjustable quarter- and half-wave plates before a polarizer. Though single-qubit quantum processes may be characterized using only 12 experimental configurations, we used 18 experimental configurations to minimize error in the SQPT data, since it was used as the benchmark for the DCQD measurements [18,19].

Measuring processes using DCQD requires entangled input states and measurements. The same down-conversion source was used for this technique, except both crystals were pumped coherently with a superposition of H and V polarizations, which created polarization entangled photon pairs [20] (only partially for some input polarizations [21]). Because of conservation of orbital angular momentum, the photons were also entangled in spatial mode [22]. Pumping the crystals with equal parts of H and V polarization prepares the following hyperentangled state [23]:

$$\frac{1}{2}(|HH\rangle - |VV\rangle) \otimes (|\circlearrowleft\circlearrowleft\rangle + |\circlearrowright\circlearrowright\rangle), \tag{2}$$

where $\circlearrowleft$ and $\circlearrowright$ represent right- and left-orbital angular momentum modes, respectively. Using a pump beam polarized at $\frac{\pi}{8}$ with respect to H, and manipulating the

polarization of both signal and idler photons using liquid crystals, it was possible to create the three additional input states required for DCQD:

$$\frac{1}{\sqrt{2}}\left(\cos\frac{\pi}{8}|HH\rangle - i\sin\frac{\pi}{8}|VV\rangle\right)\otimes(|\circlearrowleft\circlearrowleft\rangle + |\circlearrowright\circlearrowright\rangle),$$
$$\frac{1}{\sqrt{2}}\left(\cos\frac{\pi}{8}|DD\rangle - i\sin\frac{\pi}{8}|AA\rangle\right)\otimes(|\circlearrowleft\circlearrowright\rangle + |\circlearrowright\circlearrowleft\rangle),$$
$$\frac{1}{\sqrt{2}}\left(\cos\frac{\pi}{8}|LL\rangle - i\sin\frac{\pi}{8}|RR\rangle\right)\otimes(|\circlearrowleft\circlearrowleft\rangle + |\circlearrowright\circlearrowright\rangle). \quad (3)$$

Only the signal photon of each state was then propagated through the quantum process, after which we used hyperentanglement to allow us to perform polarization Bell measurements on the output states [24] [Fig. 2(a)].

The key point to performing a complete Bell measurement is the fact that a hyperentangled polarization spatial-mode Bell state may be written [24] as follows:

$$\Phi^{\pm}_{\text{spin}}\otimes\Psi^{+}_{\text{orbit}} = \frac{1}{2}(\phi^{+}_{1}\otimes\psi^{\pm}_{2} + \phi^{-}_{1}\otimes\psi^{\mp}_{2} + \psi^{+}_{1}\otimes\phi^{\pm}_{2} + \psi^{-}_{1}\otimes\phi^{\mp}_{2}),$$
$$\Psi^{\pm}_{\text{spin}}\otimes\Psi^{+}_{\text{orbit}} = \frac{1}{2}(\pm\phi^{+}_{1}\otimes\phi^{\pm}_{2} \mp \phi^{-}_{1}\otimes\phi^{\mp}_{2} \pm \psi^{+}_{1}\otimes\psi^{\pm}_{2} \mp \psi^{-}_{1}\otimes\psi^{\mp}_{2}), \quad (4)$$

where $\Phi^{\pm}$ and $\Psi^{\pm}$ represent the four two-photon Bell states for polarization (spin) and orbital angular momentum (orbit), and $\phi^{\pm}$ and $\psi^{\pm}$ are the single-photon hybrid-Bell states for both signal (1) and idler (2) photons:

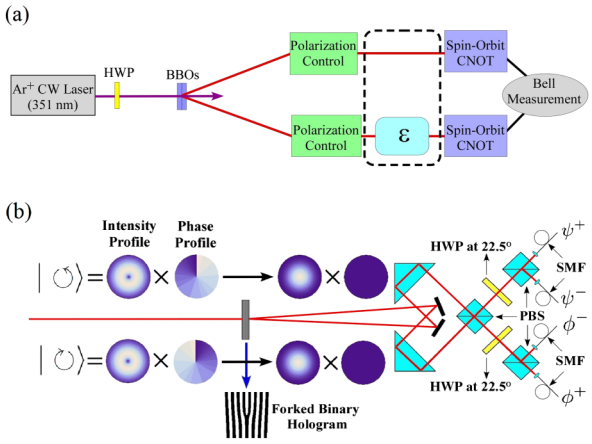

FIG. 2 (color online). (a) Experimental setup used to perform DCQD on various single-qubit quantum processes with hyperentangled photons. A half-wave plate (HWP) tunes the pump polarization to generate photon pairs for SQPT or DCQD. The DCQD input polarization states were prepared with liquid crystals (polarization control). (b) The spin-orbit CNOT gates, which were used to measure the four single-photon hybrid-entangled Bell states in Eq. (5). The outputs of a forked binary hologram are combined on a polarizing beam splitter (PBS) and then spatially filtered with single-mode fibers (SMF).

$$\psi^{\pm} = (|H\circlearrowright\rangle \pm |V\circlearrowleft\rangle)/\sqrt{2},$$
$$\phi^{\pm} = (|H\circlearrowleft\rangle \pm |V\circlearrowright\rangle)/\sqrt{2}. \quad (5)$$

Thus, determining the single-photon hybrid-entangled state of each individual photon uniquely determines the two-photon hyperentangled state. The requisite operations were implemented by interfering the ± 1-order diffracted outputs of a forked binary hologram on a polarizing beam splitter [Fig. 2(b)]. These silver-halide emulsion holograms had 33% diffraction efficiency into the first order and, when used with single-mode fibers, have the dual property of both converting different orbital angular momentum beams into Gaussian beams traveling in different directions and filtering out all but the Gaussian spatial modes [8,25]. Combined with polarizers and single-photon counters, the interferometers measure the single-photon Bell states [Eq. (5)] (Fig. 2). Thus, by detecting the outputs of each of these spin-orbit CNOT gates in coincidence, it was possible to perform a full polarization Bell measurement.

We used DCQD to characterize a wide variety of single-photon polarization processes. Pauli-matrix rotation quantum processes were applied using half-wave plates, dephasing and depolarization processes were implemented using thick birefringent quartz plates [26], and a polarization quantum process was implemented with a sheet polarizer. Tunable partial polarization or dephasing processes were implemented by placing polarization or dephasing processes in the beam path for only a fraction of the count time.

The χ matrices of each of the quantum processes were characterized using 18-experimental-configuration SQPT and 4-experimental-configuration DCQD. The χ matrices were then reconstructed using maximum likelihood techniques [27] and compared using stabilized Jamiolkowski fidelity F_J, also known as stabilized entanglement fidelity [28]. F_J was chosen over the other process fidelities because it is a stable metric which, in contrast to the more commonly used average process fidelity, can be used for all classes of quantum processes (including non-trace-preserving processes) [29].

Initial χ matrices from the two methods showed less than desired agreement due to errors in the Bell measurement. However, it has been shown that errors introduced by imperfect DCQD state preparation and faulty Bell measurement can be decoupled from the quantum process data if both error maps are well characterized [16], but characterizing the relevant two-qubit error map requires two-qubit process tomography (which in general requires quadratically more experimental configurations than a single-qubit process tomography). Fortunately, because single-qubit DCQD only requires four experimental configurations, only partial information of these error maps was required and was characterized using state tomography [11,30]. After error correction, for identical processes, the overlap between the inferred process with SQPT and

the one with DCQD was improved from a mean F_J of 89.2% to 96.0% (Fig. 3). Even after compensating these error processes, the χ matrices inferred with the two different characterization techniques are not statistically identical. This residual systematic error is due to time-dependant power fluctuations which are not corrected by this error reduction technique. Simulations of DCQD measurements with the inclusion of these power fluctuations show perfect agreement with experimental results [11].

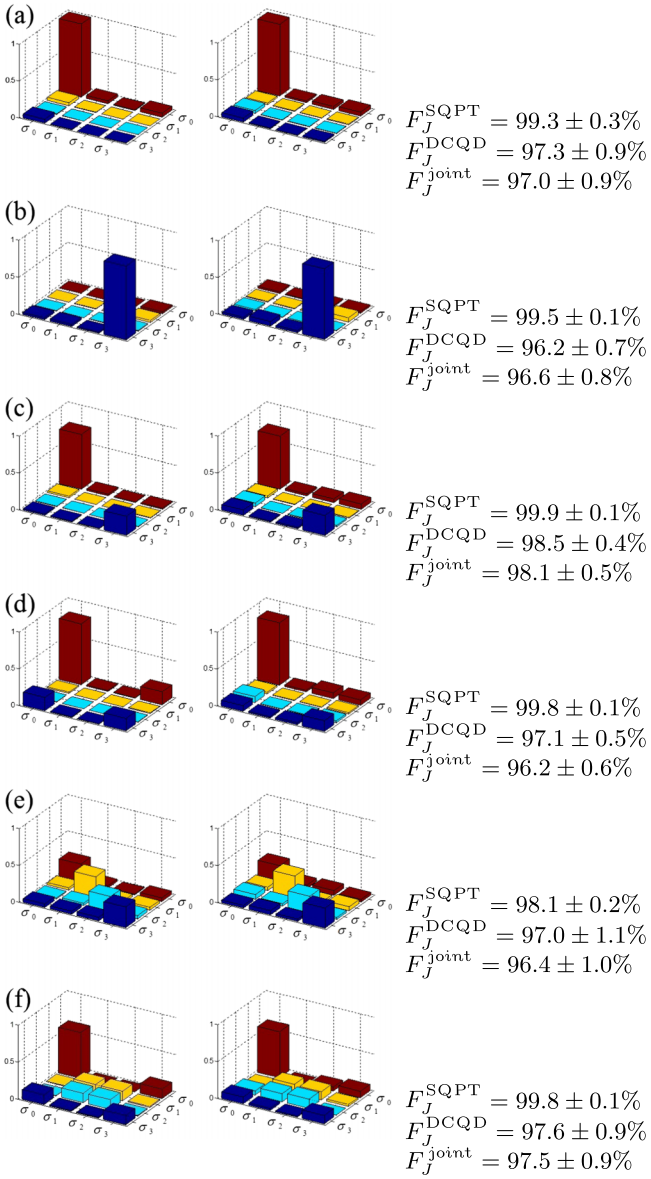

FIG. 3 (color online). Reconstructed χ matrices (absolute values of elements) from SQPT (left column) and DCQD (right column) measurements for the following: identity (a), σ_z rotation (b), partial dephasing (c), partial polarizer (d), depolarization (e), and simultaneous spin-lattice and spin-spin relaxation (f). The fidelities listed on the right compare the target process with the experimentally measured process using SQPT (F_J^{SQPT}), the target process with the experimentally measured processes using DCQD (F_J^{DCQD}), and the experimentally measured processes using SQPT and DCQD (F_J^{joint}). Uncertainties were calculated using Monte Carlo methods applied to Poissonian photon counting statistics.

It is possible to use DCQD techniques to measure significant process parameters without a complete characterization. For example, it is possible to measure both spin-lattice (T_1) and spin-spin (T_2) relaxation times using a single experimental setting [1,31,32]. Though vital in characterizing the coherence of many quantum systems (atoms, ions, quantum dots, etc.), spin-lattice relaxation is not present in most photonic systems because photons do not interact strongly with thermodynamic reservoirs nor decay to lower energy states. However, we can simulate these processes by employing a combination of time-varying polarization processes. Specifically, photons were transmitted through a thick quartz plate and a polarizer part of the time and through empty space (the identity process) the remainder. While the individual values of T_1 and T_2 have little physical significance in our optical simulation, the ratio of $R \equiv T_2$: T_1 is a measure of how coherently states evolve in this process. This ratio was measured with SQPT (1.01 ± 0.03) using an overcomplete set of 18 experimental settings and with DCQD using a *single* experimental setting input [i.e., Eq. (2)] (0.99 ± 0.06). In addition, a full 4-measurement DCQD was used to verify the ratio and to determine the off-diagonal χ-matrix elements [Fig. 3(f)].

We have implemented a powerful technique for reducing the number of experimental configurations required for characterizing quantum processes through the use of hyperentanglement-assisted Bell measurements. Furthermore, we demonstrated how these processes could be characterized even when the measurement system is subject to systematic error. In general, it should be possible to further decrease the number of experimental configurations required to characterize certain classes of quantum processes, by combining DCQD techniques with compressed sensing methods that have already been used to characterize sparse quantum states and processes with far fewer experimental configurations than would normally be required [33,34]. We have also begun studying the number of state copies DCQD needs (compared to other process tomography techniques) to statistically constrain the error of process estimation. Our current numerical simulations indicate that DCQD requires fewer state copies than SQPT to constrain the error for some classes of unitary processes; however, further investigation is required to quantify more generally when DCQD has an advantage over SQPT in terms of the required number of state copies. Nevertheless, in all cases DCQD requires 3^n times fewer experimental configurations than SQPT.

This work was funded by NSF Grant No. PHY-0903865, the ADNA/S&T-IARPA project Hyperentanglement-Enhanced Advanced Quantum Communication (NBCHC070006), QuISM MURI Program, and DARPA QuBE program.

[1] M. Mohseni and D. A. Lidar, Phys. Rev. Lett. **97**, 170501 (2006).

[2] M. Mohseni, A. T. Rezakhani, and D. A. Lidar, Phys. Rev. A **77**, 032322 (2008).

[3] A. Bendersky, F. Pastawski, and J. P. Paz, Phys. Rev. Lett. **100**, 190403 (2008).

[4] I. Ivonovîć, J. Phys. A **14**, 3241 (1981).

[5] G. M. D'Ariano, Phys. Lett. A **300**, 1 (2002).

[6] L. Vaidman and N. Yoran, Phys. Rev. A **59**, 116 (1999).

[7] Z. W. Wang, Y. S. Zhang, Y. F. Huang, X. F. Raen, and G. C. Guo, Phys. Rev. A **75**, 044304 (2007).

[8] J. T. Barreiro, T. C. Wei, and P. G. Kwiat, Nat. Phys. **4**, 282 (2008).

[9] W. T. Liu, W. Wu, P. X. Chen, C. Z. Li, and J. M. Yuan, Phys. Rev. A **77**, 032328 (2008).

[10] D. Nigg *et al.*, preceding Letter, Phys. Rev. Lett. **110**, 060403 (2013).

[11] See Supplemental Material at http://link.aps.org/supplemental/10.1103/PhysRevLett.110.060404 for details of our hyperentanglement source, error compensation strategy, and analysis of residual statistical and systematic error.

[12] I. L. Chuang and M. A Nielsen, J. Mod. Opt. **44**, 2455 (1997).

[13] It is assumed that all outcomes of projective measurements may be detected (i.e., *H&V*—and *D&A* and *L&R*—can both be simultaneously measured).

[14] J. B. Altepeter, D. Branning, E. Jeffrey, T. C. Wei, P. G. Kwiat, R. T. Thew, J. L. O'Brien, M. A. Nielsen, and A. G. White, Phys. Rev. Lett. **90**, 193601 (2003).

[15] M. A. Nielsen and I. L. Chuang, *Quantum Computation and Quantum Information* (Cambridge University Press, Cambridge, England, 2000).

[16] M. Mohseni, A. T. Rezakhani, J. T. Barreiro, P. G. Kwiat, and A. Aspuru-Guzik, Phys. Rev. A **81**, 032102 (2010).

[17] N. A. Peters, J. T. Barreiro, M. E. Goggin, T. C. Wei, and P. G. Kwiat, Phys. Rev. Lett. **94**, 150502 (2005).

[18] J. B. Altepeter, E. R. Jeffrey, P. G. Kwiat, S. Tanzilli, N. Gisin, and A. Acín, Phys. Rev. Lett. **95**, 033601 (2005).

[19] M. D. de Burgh, N. K. Langford, A. C. Doherty, and A. Gilchrist, Phys. Rev. A **78**, 052122 (2008).

[20] P. G. Kwiat, E. Waks, A. G. White, I. Appelbaum, and P. H. Eberhard, Phys. Rev. A **60**, R773 (1999).

[21] A. G. White, D. F. V. James, P. H. Eberhard, and P. G. Kwiat, Phys. Rev. Lett. **83**, 3103 (1999).

[22] A. Mair, A. Vaziri, G. Weihs, and A. Zeilinger, Nature (London) **412**, 313 (2001).

[23] In these experiments we discard all other spatial modes, e.g., both photon Gaussians.

[24] S. P. Walborn, S. Padua, and C. H. Monken, Phys. Rev. A **68**, 042313 (2003).

[25] *Optical Angular Moment*, edited by L. Allen, S. M. Barnett, and M. J. Padgett (IOP Publishing, Bristol, 2003).

[26] A. Shaham and H. S. Eisenberg, Phys. Rev. A **83**, 022303 (2011).

[27] D. F. V. James, P. G. Kwiat, W. J. Munro, and A. G. White, Phys. Rev. A **64**, 052312 (2001).

[28] $F_J = \mathrm{Tr}\{\sqrt{\sqrt{[I \otimes \epsilon_1](\rho_\Phi)}[I \otimes \epsilon_2](\rho_\Phi)\sqrt{[I \otimes \epsilon_1](\rho_\Phi)}}\}^2$, where quantum processes ϵ_1 and ϵ_2 act on one qubit of some two-qubit maximally entangled state ρ_Φ, and the fidelity is taken between the outputs of the two processes.

[29] A. Gilchrist, N. K. Langford, and M. A. Nielsen, Phys. Rev. A **71**, 062310 (2005).

[30] Preparation and measurement error maps cannot be completely characterized together because it is impossible to decouple the effects of two arbitrary error maps. For this reason, we characterized the two error maps independently from one another.

[31] M. Mohseni, A. T. Rezakhani, and A. Aspuru-Guzik, Phys. Rev. A **77**, 042320 (2008).

[32] M. Mohseni and A. T. Rezakhani, Phys. Rev. A **80**, 010101(R) (2009).

[33] D. Gross, Y. K. Liu, S. T. Flammia, S. Becker, and J. Eisert, Phys. Rev. Lett. **105**, 150401 (2010).

[34] A. Shabani, R. L. Kosut, M. Mohseni, H. Rabitz, M. A. Broome, M. P. Almeida, A. Fedrizzi, and A. G. White, Phys. Rev. Lett. **106**, 100401 (2011); A. Shabani, M. Mohseni, S. Lloyd, R. L. Kosut, and H. Rabitz, Phys. Rev. A **84**, 012107 (2011).